Catalysis Science & Technology

Volume 15
Number 12
21 June 2025
Pages 3455–3774

rsc.li/catalysis

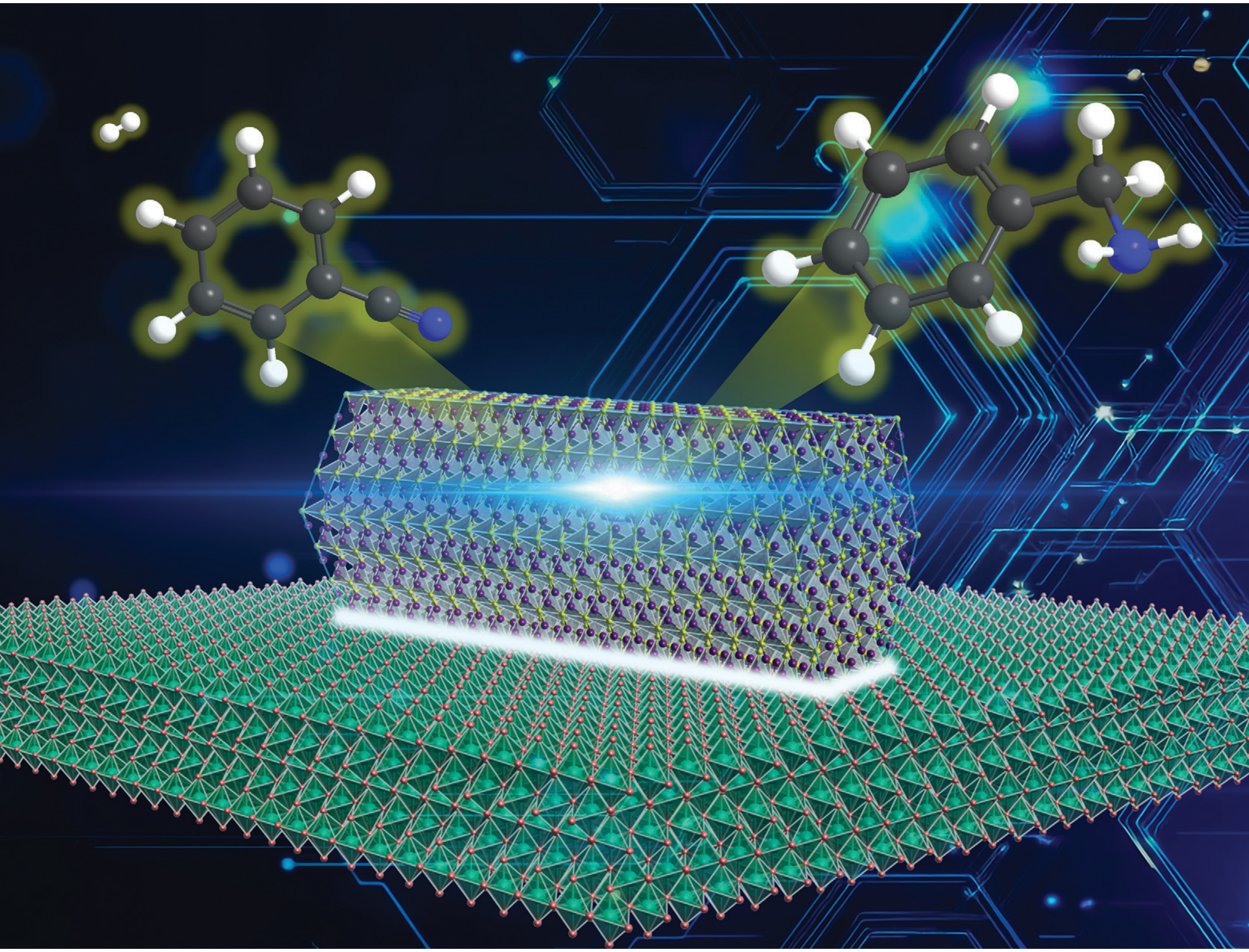

ISSN 2044-4761

ROYAL SOCIETY
OF **CHEMISTRY**

PAPER
Takato Mitsudome *et al.*
Green synthesis of iron phosphide nanoparticles with high catalytic activity for liquid-phase nitrile hydrogenation

Catalysis
Science &
Technology

ROYAL SOCIETY
OF CHEMISTRY

PAPER

View Article Online
View Journal | View Issue

Check for updates

Cite this: *Catal. Sci. Technol.*, 2025, **15**, 3544

Green synthesis of iron phosphide nanoparticles with high catalytic activity for liquid-phase nitrile hydrogenation†

Tomohiro Tsuda,[a] Shintaro Toyoda,[a] Hiroya Ishikawa,[a] Sho Yamaguchi,[ab] Tomoo Mizugaki[abc] and Takato Mitsudome *[abd]

Received 28th January 2025,
Accepted 20th April 2025

DOI: 10.1039/d5cy00112a

rsc.li/catalysis

Owing to the natural abundance, cost-effectiveness, and minimal environmental impact of iron, iron-based catalysts are widely recognized as promising. In this context, iron phosphide nanoparticles have recently attracted attention as a distinctive class of air-stable and highly active iron-based catalysts for liquid-phase hydrogenation reactions as well as electrochemical reactions. However, conventional synthesis methods typically require highly toxic iron and phosphorus sources such as $Fe(CO)_5$ and phosphine derivatives, posing severe practical and environmental concerns. In this study, we developed a safer and more environmentally friendly method for the synthesis of iron phosphide nanoparticles by utilizing iron carboxylates as non-toxic and readily available iron precursors and triphenylphosphite as a comparatively benign phosphorus source. This approach eliminates the need for hazardous reagents while allowing precise control over particle size and phase formation. By optimizing the iron precursor type, heating duration, temperature, and phosphorus amount, we selectively synthesized the Fe_2P phase under mild solvothermal conditions. Furthermore, the resulting Fe_2P nanoparticles exhibited twice the catalytic activity of those previously synthesized from $Fe(CO)_5$ in the liquid-phase hydrogenation of nitriles, highlighting the effectiveness of this green synthetic strategy. This method provides a practical and sustainable approach for the synthesis of catalytically active iron phosphide nanoparticles, potentially enabling their broader application in various catalytic and energy-related fields.

Introduction

Replacing noble metals in catalysts with non-precious alternatives is a critical step toward achieving sustainable catalytic systems. Among these alternatives, iron is particularly promising due to its abundance, cost-effectiveness, and low environmental impact.[1–3] However, iron nanoparticles (Fe NPs) have predominantly been employed in industrial applications involving high-temperature gas-phase hydrogenation reactions of small molecules, such as nitrogen and carbon monoxide.[4–6] Their broader application, particularly to lower-temperature liquid-phase hydrogenation reactions, has been severely limited by their low catalytic activity and susceptibility to oxidative deactivation.[7,8] Nevertheless, recent advancements in catalyst design have extended the utility of iron catalysts to liquid-phase reactions under milder conditions, enabling transformations of larger and more structurally complex substrates.[9–16] In this context, we have reported that rod-shaped iron phosphide nanoparticles (Fe_2P NPs) function as a highly active and reusable heterogeneous catalyst for the liquid-phase hydrogenation reactions.[17] The strong Fe–P covalent bonding in Fe_2P NPs imparts exceptional air stability, addressing a long-standing limitation of conventional iron-based catalysts. This stability, combined with high catalytic activity, demonstrates the significant potential of iron-based catalysts for sustainable chemical processes.

Nanosized iron phosphides (Fe_xP NPs, $x = 1$, or 2) have attracted increased attention as catalysts for liquid-phase hydrogenation reactions as well as electrochemical applications.[18,19] The synthesis of Fe_xP NPs has been investigated using solid-phase[20–26] and liquid-phase methods[17,27–38] (see Table S1† for a summary of previously reported synthetic methods). The solid-phase synthesis typically employs highly reactive inorganic phosphorus sources, such as NaH_2PO_2 and Na_3P, which decompose into PH_3 and subsequently react with iron

---

[a] Department of Materials Engineering Science, Graduate School of Engineering Science, Osaka University, 1-3 Machikaneyama, Toyonaka, Osaka, 560-8531, Japan. E-mail: mitsudom@cheng.es.osaka-u.ac.jp
[b] Innovative Catalysis Science Division, Institute for Open and Transdisciplinary Research Initiatives (ICS-OTRI), Osaka University, Suita, Osaka, 565-0871, Japan
[c] Research Center for Solar Energy Chemistry, Graduate School of Engineering Science, Osaka University, 1-3 Machikaneyama, Toyonaka, Osaka, 560-8531, Japan
[d] Precursory Research for Embryonic Science and Technology (PRESTO), Japan Science and Technology Agency (JST), 4-1-8 Honcho, Kawaguchi, Saitama, 333-0012, Japan

† Electronic supplementary information (ESI) available. See DOI: **https://doi.org/10.1039/d5cy00112a**

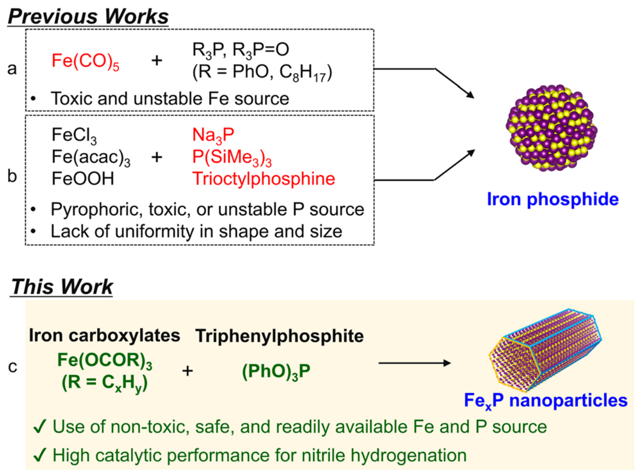
Previous Works
a
Fe(CO)5
+
R3P, R3P=O
(R = PhO, C8H17)
• Toxic and unstable Fe source
b
FeCl3
Fe(acac)3
FeOOH
+
Na3P
P(SiMe3)3
Trioctylphosphine
• Pyrophoric, toxic, or unstable P source
• Lack of uniformity in shape and size
Iron phosphide
This Work
c
Iron carboxylates
Triphenylphosphite
Fe(OCOR)3
(R = CxHy)
+
(PhO)3P
FexP nanoparticles
✓ Use of non-toxic, safe, and readily available Fe and P source
✓ High catalytic performance for nitrile hydrogenation

Fig. 1 Comparison of liquid-phase synthesis of iron phosphide nanoparticles using (a and b) conventional methods and (c) the method developed in this study.

precursors, including iron salts, hydroxides, or oxides. While this strategy is suitable for large-scale synthesis of iron phosphides, it requires relatively high temperature (typically exceeding 400 °C) and/or highly toxic, corrosive, and explosive phosphorus sources. In contrast, liquid-phase methods can be operated under milder conditions utilizing Fe(CO)$_5$ and organic phosphorous compounds (Fig. 1a). This approach enables the selective synthesis of Fe$_x$P NPs with controlled shapes, sizes, and compositions.[17,27–34] However, the inherent toxicity and air sensitivity of Fe(CO)$_5$ still present significant safety concerns, limiting its practical application in both laboratories and industries. To address these limitations, several studies have explored alternative approaches to replace Fe(CO)$_5$ with less toxic and more stable iron precursors, such as FeCl$_3$, Fe(acac)$_3$, and FeOOH (Fig. 1b).[35–38] Although these strategies have successfully synthesized FeP, they remain dependent on pyrophoric, toxic, or air unstable phosphorus sources such as Na$_3$P, P(SiMe$_3$)$_3$, or trioctylphosphine. Furthermore, the resulting iron phosphides often lack uniformity in shape and size. Consequently, the development of a safe, accessible, and precisely controllable method for the synthesis of nanosized iron phosphides is not only a critical area of research but also essential for advancing their practical applications.

In this study, we developed a novel liquid-phase synthesis of Fe$_x$P NPs utilizing iron carboxylates and triphenylphosphite (TPP) as non-toxic, safe, and readily available iron and phosphorus sources (Fig. 1c). This method provides a straightforward and clean route to synthesize Fe$_x$P NPs. Furthermore, the catalytic activity of the synthesized Fe$_x$P NPs was evaluated in the hydrogenation of benzonitrile.

Results and discussion

Preparation and characterization

Iron carboxylates were synthesized according to previously reported methods (see details in the ESI†).[39] The example of the synthesis of iron oleate (Fe–Ol) is as follows. FeCl$_3$·6H$_2$O was dissolved in distilled water in a round-bottom flask, and sodium oleate, ethanol, and hexane were added. The flask was purged with Ar gas, heated to 70 °C, and stirred for 4 h. The mixture was then washed with distilled water using a separatory funnel, and the organic phase was extracted. After evaporating hexane in the organic phase, a reddish-brown waxy Fe–Ol was obtained. The result of attenuated total reflection Fourier transform infrared (ATR-FTIR) spectrum was consistent with the inclusion of oleate structure in Fe–Ol (Fig. S1†). Similarly, by substituting sodium oleate with sodium erucate, sodium stearate, and sodium laurate, iron erucate (Fe–Er), iron stearate (Fe–St), and iron laurate (Fe–La) were synthesized, respectively. Iron acetate (Fe–Ac) was used as a commercially available iron precursor.

The standard preparation method of the Fe$_x$P NPs from the iron carboxylates is as follows. TPP and hexadecylamine were added to a Schlenk tube, and the mixture was stirred under vacuum at 120 °C for 30 min. The prepared iron carboxylate was then introduced, and the mixture was heated to 320 °C at a rate of 50 °C min^{-1} and then held constant for 4 h. The resulting black colloidal solution was centrifuged to collect the product, which was then washed with acetone and chloroform to obtain black nanoparticles. Fe$_x$P NPs synthesized from Fe–Ol, Fe–Er, Fe–St, Fe–La, and Fe–Ac are denoted as Fe$_x$P–Ol, Fe$_x$P–Er, Fe$_x$P–St, Fe$_x$P–La, and Fe$_x$P–Ac, respectively.

Fig. 2 shows characterization results of the prepared Fe$_x$P–Ol. The X-ray diffraction (XRD) revealed three characteristic peaks at 2θ = 40.1°, 52.1°, and 54.2°, which were assigned to the $(2\bar{1}\bar{1}1)$, (0002), and $(30\bar{3}0)$ crystalline planes of hexagonal Fe$_2$P (JCPDS card number 51-0943), respectively (Fig. 2a). Elemental analysis of Fe$_x$P–Ol using inductively coupled plasma-atomic emission spectrometry (ICP-AES) revealed that the molar ratio of Fe to P was close to 2 : 1 (Table S2†). Representative transmission electron microscope (TEM) image of Fe$_x$P–Ol shows rod-like structure (Fig. 2b). A size distribution histogram indicates that Fe$_x$P–Ol is regular nanorods with an average length of 50.0 nm and width of 8.8 nm (Fig. 2c). This is almost two times longer than the previously reported approximately 26.5 nm for Fe$_2$P NPs synthesized from Fe(CO)$_5$.[17] These observations indicate that crystalline Fe$_2$P nanoparticles can be selectively synthesized. Fe–Ol may serve as an effective iron precursor due to their decomposition temperature (around 300 °C),[40] which is close to our solvothermal conditions. Fig. 2d shows the X-ray absorption near-edge structure (XANES) spectrum of Fe$_x$P–Ol after exposure to air along with those of Fe foil, Fe–Ol, and Fe$_2$O$_3$. The absorption edge energy of Fe$_x$P–Ol is considerably lower than that of Fe$_2$O$_3$ and Fe–Ol, and very close to that of Fe foil. This air stability is consistent with previously reported finding[17] and is in stark contrast to the air instability of conventional Fe NPs.

To demonstrate the generality of this facile synthesis of Fe$_x$P NPs from iron carboxylates, other carboxylate complexes, Fe–Er, Fe–St, Fe–La, and Fe–Ac were investigated,

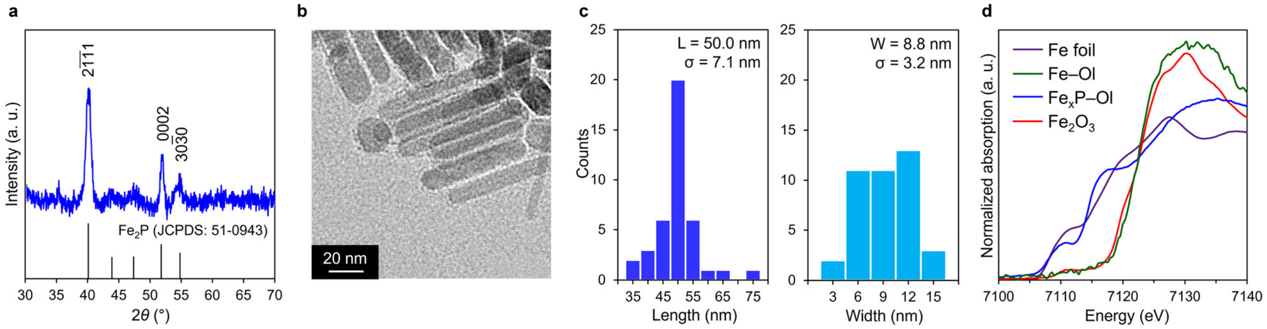

Fig. 2 The characterization results of Fe$_x$P–Ol. (a) XRD pattern of Fe$_x$P–Ol (black bars below the pattern show the diffraction peaks referring to JCPDS card number 51-0943). (b) TEM image and (c) size distribution histogram of Fe$_x$P–Ol. (d) Fe K-edge XANES spectrum of Fe$_x$P–Ol with Fe foil, Fe–Ol, and Fe$_2$O$_3$ as references.

and the results are summarized in Fig. 3. XRD patterns reveal that peaks were attributed to Fe$_2$P or FeP (JCPDS card number 89-2746) without any other iron compounds such as iron oxides and iron (metal), demonstrating selective synthesis of Fe$_x$P (Fig. 3a–d). Iron precursors with long-chain alkyl groups (*i.e.*, Fe–Er and Fe–St) selectively provided the Fe$_2$P phase, similar to the result of Fe–Ol (Fig. 3a and b). On the other hand, the obtained iron phosphide was found to be a mixture of Fe$_2$P and FeP using Fe$_x$P–La or Fe$_x$P–Ac (Fig. 3c and d). Fig. 3e–h show the TEM images of the synthesized Fe$_x$P. While similar rod shape was seen from Fe$_x$P–Er and Fe$_x$P–St, their mean sizes were considerably large (>80 nm) (Fig. 3i and j). In the case of Fe$_x$P–La, rod-like structures were also observed (inset of Fig. 3g), but most of the nanoparticles were spherical with a mean size of 9.4 nm (Fig. 3k). Rod-like structures were not observed in Fe$_x$P–Ac and spherical nanoparticles with a mean size of 4.8 nm were selectively obtained (Fig. 3l). These results indicate that the formation of rod-like Fe$_2$P is dominant when the alkyl chain is long, while FeP nanoparticles tend to be obtained from iron carboxylates with relatively short alkyl chains. Control experiments using FeOOH, FeCl$_3$·6H$_2$O, and Fe(acac)$_3$ as alternative iron sources under similar preparation conditions did not yield any iron phosphides, with FeOOH leading to the formation of Fe$_2$O$_3$, and FeCl$_3$·6H$_2$O and Fe(acac)$_3$ resulting in amorphous materials (Fig. S2†). This finding

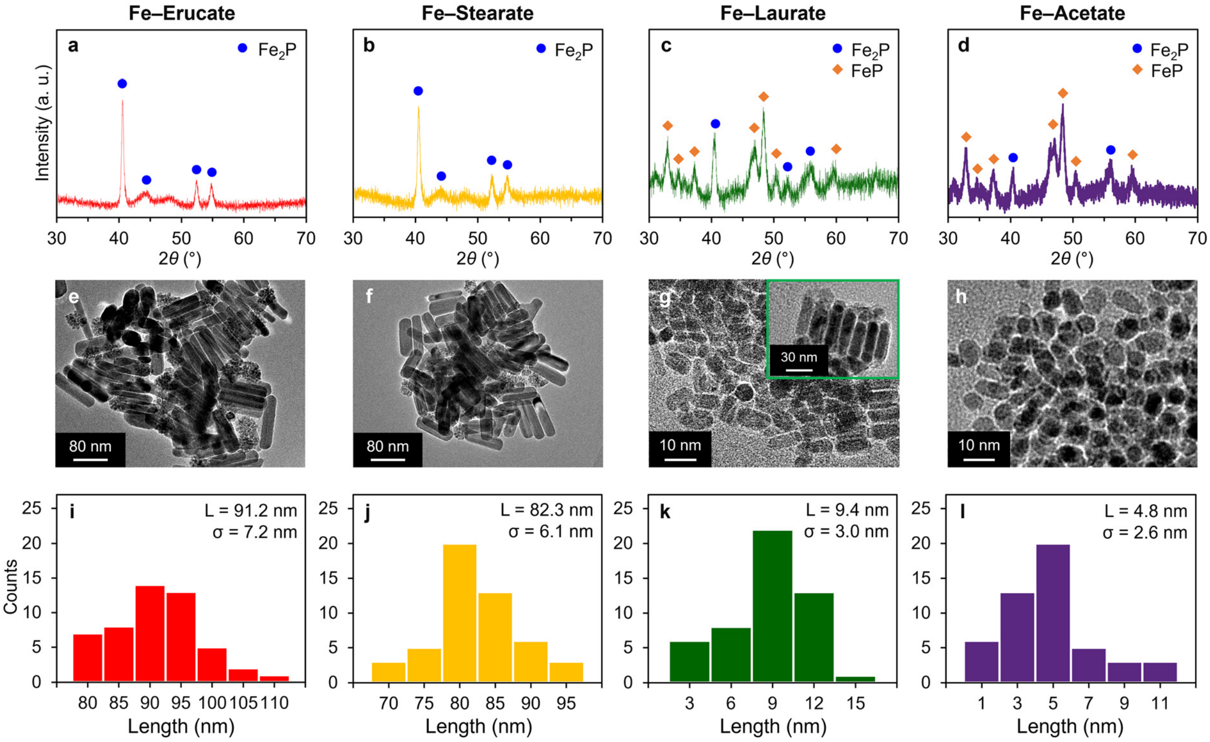

Fig. 3 XRD patterns of (a) Fe$_x$P–Er, (b) Fe$_x$P–St, (c) Fe$_x$P–La, and (d) Fe$_x$P–Ac. TEM images and size distribution histograms of (e and i) Fe$_x$P–Er, (f and j) Fe$_x$P–St, (g and k) Fe$_x$P–La, and (h and l) Fe$_x$P–Ac.

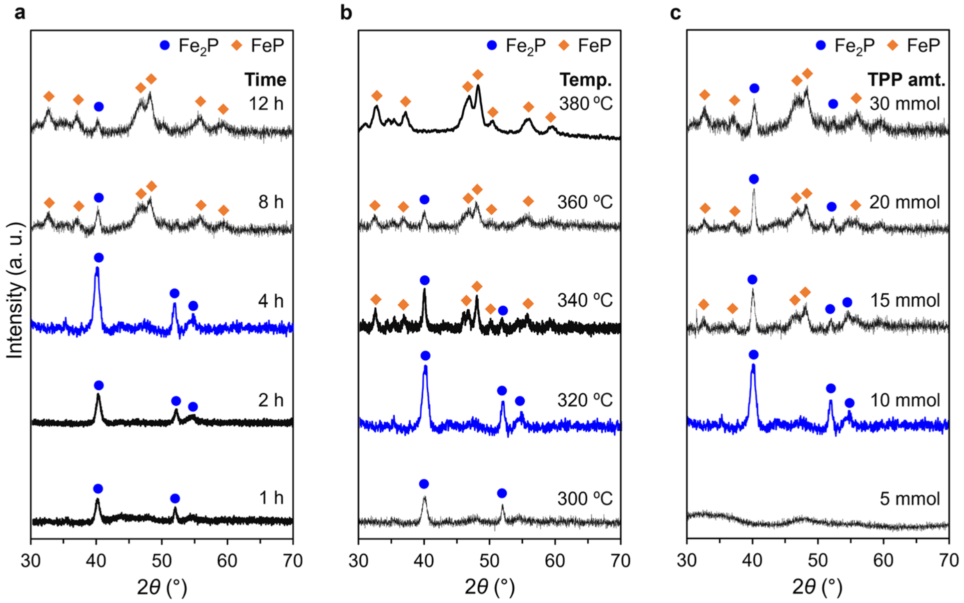

Fig. 4 XRD patterns of Fe_xP–Ol obtained from different (a) heating time, (b) heating temperature, and (c) TPP amount. Synthesis conditions: Fe–Ol (1 mmol), hexadecylamine (10 mmol), TPP (5–30 mmol), heating temperature (300–380 °C), and time (1–12 h).

highlights the critical role of iron carboxylates in enabling the synthesis of iron phosphides.

The influence of synthesis conditions on the composition of Fe_xP was systematically investigated using Fe_xP–Ol as a model system. The XRD patterns in Fig. 4 illustrate the effects of heating time, heating temperature, and amount of phosphorus source on the resulting phases. The impact of heating time was first examined at a constant temperature of 320 °C (Fig. 4a). Small peaks in the XRD pattern at 1 h suggested poorly crystalline Fe_2P formation. Extending the duration to 4 h improved crystallinity with only peaks attributable to Fe_2P, suggesting the selective formation of Fe_2P. By 8 h, FeP peaks emerged alongside Fe_2P, signifying a phase coexistence. At 12 h, FeP became dominant, as evidenced by its strong XRD peaks. Next, the effect of heating temperature was explored (Fig. 4b). At 300 °C, Fe_2P was the predominant phase, consistent with observations at 320 °C. Increasing the temperature to 340 °C facilitated the formation of FeP, while the Fe_2P phase was reduced. At 360 °C, the Fe_2P peak intensity further decreased, and at 380 °C, the FeP phase was selectively obtained, demonstrating the temperature's decisive role in phase control. Finally, the influence of TPP amount was assessed (Fig. 4c). When 5 mmol of TPP was used, no Fe_xP phases were detected. Increasing the amount of TPP to 10 mmol led to the selective synthesis of Fe_2P. Further increasing the TPP amount resulted in the formation of FeP with a slight decrease in Fe_2P peak intensity. However, complete conversion to FeP was not achieved even at the highest TPP amount tested. This finding highlights the importance of fine-tuning factors such as heating time, temperature, and phosphorus amount. Notably, Fe_2P and FeP can be selectively synthesized by carefully controlling the heating temperature, with Fe_2P at 320 °C and FeP at 380 °C.

Catalyst performance

Finally, the catalytic activities of the synthesized Fe_xP NPs were evaluated in nitrile hydrogenation, which is a reaction of significant industrial relevance for the production of primary amines. Although numerous catalysts based on precious and non-precious metals have been developed for such reactions, iron catalysts remain scarce.[11,17] The catalytic activity was assessed using benzonitrile (**1**) as a model substrate under 3.8 MPa of H_2 and 0.2 MPa of NH_3 at 180 °C for 2 h.

As shown in Fig. 5, Fe_xP–Ol and Fe_xP–La promoted the hydrogenation of **1** to give benzylamine (**2**) in 36% and 14% yields, respectively (see Table S3 for product selectivity and Fig. S3† for proposed reaction path). In contrast, other Fe_xP NPs, including Fe_xP–St, Fe_xP–Er, and Fe_xP–Ac exhibited significantly low activities. The catalytic activity demonstrates that Fe_xP–Ol exhibited approximately twice the yield of previously reported Fe_2P NPs from $Fe(CO)_5$ (36% *vs.* 19%),[17] highlighting the potential of environmentally benign iron carboxylates as viable precursors for active iron phosphide catalysts (see Table S4† for TOF comparison). The spent Fe_xP–Ol catalyst was easily recovered under ambient conditions through centrifugation, and representative TEM image showed no significant changes in the morphology of Fe_xP–Ol (Fig. S4†). Additionally, among Fe_xP–Ol synthesized from different heating temperature in Fig. 4b, Fe_xP–Ol prepared at 320 °C exhibited the highest activity for this reaction (Table S5†). To elucidate the higher activity of Fe_xP–Ol and Fe_xP–La, further investigation is required; however, the selective formation of rod-shaped Fe_2P may play a crucial role; specific crystal planes exposed on these structures may contribute distinct catalytic properties.

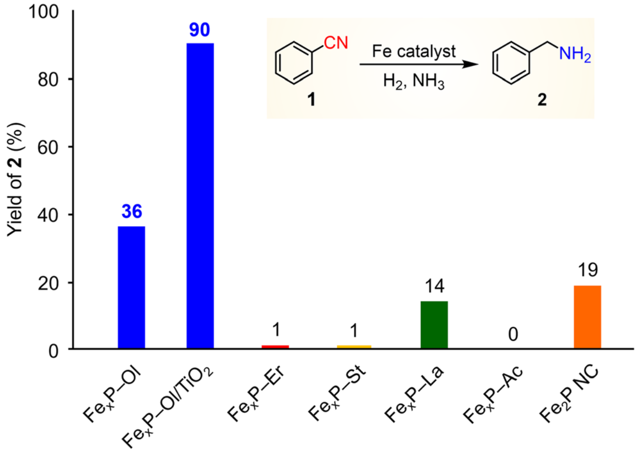

Fig. 5 Catalytic performances of various Fe_xP nanoparticles for hydrogenation of **1**. Reaction conditions: Fe_xP (7.6 mol%), **1** (0.5 mmol), 2-propanol (2 mL), H_2 gas (3.8 MPa), NH_3 gas (0.2 MPa), 180 °C, and 2 h. Yield was determined by gas chromatography (GC) using an internal standard technique.

Furthermore, the immobilization of Fe_xP–Ol nanoparticles on a TiO_2 support was attempted to improve their catalytic efficiency (see Fig. S5 and S6† for characterization of Fe_xP–Ol/TiO_2). Our previous study has demonstrated that Fe_2P NPs exhibit remarkable air stability, allowing straightforward immobilization on metal oxide supports, among which TiO_2 was particularly effective in significantly enhancing their catalytic activity in nitrile hydrogenations, presumably due to electron donation from TiO_2 to Fe_2P.[17] This approach led to a significant improvement on the yield of **2**, reaching 90% (Fig. 5). In addition, Fe_xP–Ol/TiO_2 system was suitable for use with different types of nitriles, such as heterocyclic and aliphatic nitriles (Fig. S7†). These results clearly demonstrate the successful synthesis of a highly active iron-based catalyst for liquid-phase hydrogenation reactions.

Conclusion

In this study, we developed a green and practical route for synthesizing iron phosphide nanoparticles. This method utilizes various iron carboxylates, which are safe, economical, and readily available iron sources. The Fe_2P and FeP phases are selectively synthesized by optimizing the iron precursor, heating temperature, time, and amount of phosphorus. Moreover, it was found that Fe_2P synthesized from the iron-oleate and iron-laurate complexes exhibited high catalytic activity for liquid-phase nitrile hydrogenation. This strategy provides a facile and clean approach for the synthesis of iron phosphide nanoparticles. This synthetic methodology may serve as a basis for the preparation of other metal phosphides with tailored properties, enabling their utilization in diverse catalytic and energy-related applications. Further investigation into the correlation between structural characteristics and catalytic performance is anticipated to facilitate the development of efficient and sustainable catalytic systems.

Data availability

The main data generated in this study are provided in the paper and the ESI.† Additional data are available from the corresponding authors upon reasonable request.

Author contributions

T. T. and S. T. designed the experiments, conducted the catalytic activity tests, and characterized the catalysts. H. I., S. Y., and T. Miz. discussed the experiments and results. T. Mit. directed the project and wrote the manuscript with input from all the authors. All authors commented critically on the manuscript and approved the final manuscript.

Conflicts of interest

There are no conflicts to declare.

Acknowledgements

This work was supported by JSPS KAKENHI grants 23H01761, 24K01255, and the JST PRESTO grant JPMJPR21Q9. It was also partially supported by JST-CREST grant JPMJCR21L5. We thank Dr. Kazuo Kato (SPring-8) for conducting the XAFS measurements (2023B1646). Part of the experimental analysis was supported by the "Advanced Research Infrastructure for Materials and Nanotechnology in Japan (ARIM)" (grant no. JPMXP1222HK0062) of the Ministry of Education, Culture, Sports, Science, and Technology (MEXT), Japan. This work was the result of using shared research equipment from the MEXT Project for promoting the public utilization of advanced research infrastructure (program for supporting construction of core facilities) (grant no. JPMXS0441200023 and JPMXS0441200024).

Notes and references

1 D. Wei and C. Darcel, *Chem. Rev.*, 2019, **119**, 2550–2610.
2 M. Armbrüster, K. Kovnir, M. Friedrich, D. Teschner, G. Wowsnick, M. Hahne, P. Gille, L. Szentmiklósi, M. Feuerbacher, M. Heggen, F. Girgsdies, D. Rosenthal, R. Schlögl and Y. Grin, *Nat. Mater.*, 2012, **11**, 690–693.
3 I. Bauer and H.-J. Knölker, *Chem. Rev.*, 2015, **115**, 3170–3387.
4 J.-C. Liu, X.-L. Ma, Y. Li, Y.-G. Wang, H. Xiao and J. Li, *Nat. Commun.*, 2018, **9**, 1610.
5 T. Kandemir, M. E. Schuster, A. Senyshyn, M. Behrens and R. Schlögl, *Angew. Chem., Int. Ed.*, 2013, **52**, 12723–12726.
6 Y. Cheng, J. Lin, K. Xu, H. Wang, X. Yao, Y. Pei, S. Yan, M. Qiao and B. Zong, *ACS Catal.*, 2016, **6**, 389–399.
7 A. Welther and A. Jacobi von Wangelin, *Curr. Org. Chem.*, 2013, **17**, 326–335.
8 Z. H. Farooqi, R. Begum, K. Naseem, W. Wu and A. Irfan, *Catal. Rev.: Sci. Eng.*, 2022, **64**, 286–355.
9 W. Li, J. Rabeah, F. Bourriquen, D. Yang, C. Kreyenschulte, N. Rockstroh, H. Lund, S. Bartling, A.-E. Surkus, K. Junge, A. Brückner, A. Lei and M. Beller, *Nat. Chem.*, 2022, **14**, 334–341.

10 J. F. Sonnenberg, N. Coombs, P. A. Dube and R. H. Morris, *J. Am. Chem. Soc.*, 2012, **134**, 5893–5899.

11 V. G. Chandrashekhar, T. Senthamarai, R. G. Kadam, O. Malina, J. Kašlík, R. Zbořil, M. B. Gawande, R. V. Jagadeesh and M. Beller, *Nat. Catal.*, 2022, **5**, 20–29.

12 C. Bäumler, C. Bauer and R. Kempe, *ChemSusChem*, 2020, **13**, 3110–3114.

13 Z. Ma, C. Kuloor, C. Kreyenschulte, S. Bartling, O. Malina, M. Haumann, P. W. Menezes, R. Zbořil, M. Beller and R. V. Jagadeesh, *Angew. Chem., Int. Ed.*, 2024, **63**, e202407859.

14 Y. Kita, N. Yanagisawa, M. Arai, K. Kamata and M. Hara, *Catal. Sci. Technol.*, 2024, **14**, 5430–5438.

15 R. V. Jagadeesh, A.-E. Surkus, H. Junge, M.-M. Pohl, J. Radnik, J. Rabeah, H. Huan, V. Schünemann, A. Brückner and M. Beller, *Science*, 2013, **342**, 1073–1076.

16 M. Tejeda-Serrano, J. R. Cabrero-Antonino, V. Mainar-Ruiz, M. López-Haro, J. C. Hernández-Garrido, J. J. Calvino, A. Leyva-Pérez and A. Corma, *ACS Catal.*, 2017, **7**, 3721–3729.

17 T. Tsuda, M. Sheng, H. Ishikawa, S. Yamazoe, J. Yamasaki, M. Hirayama, S. Yamaguchi, T. Mizugaki and T. Mitsudome, *Nat. Commun.*, 2023, **14**, 5959.

18 S. Xu, H. Zhao, T. Li, J. Liang, S. Lu, G. Chen, S. Gao, A. M. Asiri, Q. Wu and X. Sun, *J. Mater. Chem. A*, 2020, **8**, 19729–19745.

19 L. Tian, X. Yan and X. Chen, *ACS Catal.*, 2016, **6**, 5441–5448.

20 J. Tian, Q. Liu, Y. Liang, Z. Xing, A. M. Asiri and X. Sun, *ACS Appl. Mater. Interfaces*, 2014, **6**, 20579–20584.

21 D. Y. Chung, S. W. Jun, G. Yoon, H. Kim, J. M. Yoo, K.-S. Lee, T. Kim, H. Shin, A. K. Sinha, S. G. Kwon, K. Kang, T. Hyeon and Y.-E. Sung, *J. Am. Chem. Soc.*, 2017, **139**, 6669–6674.

22 F. Wu, Z. Chen, H. Wu, F. Xiao, S. Du, C. He, Y. Wu and Z. Ren, *ACS Sustainable Chem. Eng.*, 2019, **7**, 12741–12749.

23 T. Zhang, T. Yang, B. Li, S. Wei and W. Gao, *Appl. Surf. Sci.*, 2022, **597**, 153662.

24 F.-X. Ma, C.-Y. Xu, F. Lyu, B. Song, S.-C. Sun, Y. Y. Li, J. Lu and L. Zhen, *Adv. Sci.*, 2019, **6**, 1801490.

25 L. Song, S. Zhang and Q. Ma, *Chem. Eng. J.*, 2015, **281**, 281–285.

26 A. L. Hector and I. P. Parkin, *J. Mater. Chem.*, 1994, **4**, 279–283.

27 C. Qian, F. Kim, L. Ma, F. Tsui, P. Yang and J. Liu, *J. Am. Chem. Soc.*, 2004, **126**, 1195–1198.

28 J. Park, B. Koo, Y. Hwang, C. Bae, K. An, J.-G. Park, H. M. Park and T. Hyeon, *Angew. Chem., Int. Ed.*, 2004, **43**, 2282–2285.

29 J. Park, B. Koo, K. Y. Yoon, Y. Hwang, M. Kang, J.-G. Park and T. Hyeon, *J. Am. Chem. Soc.*, 2005, **127**, 8433–8440.

30 G. Cho, Y. Park, H. Kang, Y. Hong, T. Lee and D.-H. Ha, *Appl. Surf. Sci.*, 2020, **510**, 145427.

31 T. Chouki, M. Machreki and S. Emin, *Int. J. Hydrogen Energy*, 2020, **45**, 21473–21482.

32 Y. Park, H. Kim, T. Lee, Y.-K. Hong, W. Jeong, S.-K. Kim and D.-H. Ha, *Chem. Eng. J.*, 2022, **431**, 133217.

33 E. Muthuswamy, P. R. Kharel, G. Lawes and S. L. Brock, *ACS Nano*, 2009, **3**, 2383–2393.

34 J. Liu, M. Meyns, T. Zhang, J. Arbiol, A. Cabot and A. Shavel, *Chem. Mater.*, 2018, **30**, 1799–1807.

35 G. Yunle, G. Fan, Q. Yitai, Z. Huagui and Y. Ziping, *Mater. Res. Bull.*, 2002, **37**, 1101–1105.

36 D. Ahluwalia, A. Varshney, S. Kumar, A. Kumar, S. G. Warkar, N. Singh and P. Dubey, *Inorg. Nano-Met. Chem.*, 2020, **50**, 908–913.

37 S. C. Perera and S. L. Brock, *Mater. Res. Soc. Symp. Proc.*, 2002, **755**, 129–134.

38 M. Adhikari, S. Sharma, E. Echeverria, D. N. McIlroy and Y. Vasquez, *ACS Nanosci. Au*, 2023, **3**, 491–499.

39 L. M. Bronstein, X. Huang, J. Retrum, A. Schmucker, M. Pink, B. D. Stein and B. Dragnea, *Chem. Mater.*, 2007, **19**, 3624–3632.

40 J. Park, K. An, Y. Hwang, J.-G. Park, H.-J. Noh, J.-E. Kim, J.-G. Park, N.-M. Hwang and T. Hyeon, *Nat. Mater.*, 2004, **3**, 891–895.